Sputtering of nanostructured tungsten and comparison to modelling with TRI3DYN

Stadlmayr, R.; Szabo, P. S.; Mayer, D.; Cupak, C.; Dittmar, T.; Bischoff, L.; Möller, S.; Rasinski, M.; Wilhelm, R. A.; Möller, W.; Aumayr, F.;

Originally published:

February 2020

Journal of Nuclear Materials 532(2020), 152019-1-152019-9

DOI: https://doi.org/10.1016/j.jnucmat.2020.152019

Sputtering of Nanostructured Tungsten and Comparison to Modelling with TRI3DYN

R. Stadlmayr[a,*], P.S. Szabo[a], D. Mayer[a], C. Cupak[a], T. Dittmar[c], L. Bischoff[d], T. Schwarz-Selinger[b], W. Möller[d], F. Aumayr[a]

[a] *Institute of Applied Physics, TU Wien, Fusion@ÖAW, Wiedner Hauptstraße 8-10, 1040 Vienna, Austria*
[b] *Max-Planck-Institut für Plasmaphysik, Bolzmannstraße 2, 85748 Garching, Germany*
[c] *Forschungszentrum Jülich GmbH, Institut für Energie und Klimaforschung—Plasmaphysik, 52425 Jülich, Germany*
[d] *Institute of Ion Beam Physics and Materials Research, Helmholtz-Zentrum Dresden-Rossendorf, Bautzner Landstraße 400, 01328 Dresden, Germany*

Abstract

He-induced nanostructured tungsten (so called W-fuzz) was bombarded with Ar ions under 60 degree and the dynamic erosion behaviour experimentally investigated. By using a highly sensitive quartz-crystal-microbalance technique in a particle catcher configuration the sputtered particles distribution of W-fuzz could be evaluated. In contrast to a flat sample, where sputtered particles are emitted primarily in forward direction, we find that W-fuzz samples emit sputtered particles preferably in backward direction (i.e. in the direction of the incident ion beam). After continuous Ar irradiation of a W-fuzz sample the distribution approaches that of a flat sample. In addition to experimental data we also show modelling results obtained with a state-of-the-art Monte-Carlo (MC) binary collision approximation (BCA) code TRI3DYN in full 3D. Surface morphology changes as monitored by SEM as well as the dynamic sputtering behaviour can be well reproduced by the full 3D MC-BCA code.

Keywords: Erosion, Quartz crystal microbalance, TRI3DYN, Surface roughness, Sputtering, nanostructured tungsten, W-fuzz

*Corresponding author
Email address: stadlmayr@iap.tuwien.ac.at (R. Stadlmayr)

1. Introduction

The first wall in a nuclear fusion device is exposed to very high heat loads and continuous particle bombardment from the fusion fuel. Therefore the key parameters of a plasma facing material (PFM) are a high melting point, low fuel retention and a low sputtering yield. Tungsten fulfills all these characteristics and is therefore the material of choice in present day fusion reactors [1, 2]. However, under special conditions a tungsten surface can form nanometer-sized fibreform structures, also called tungsten-fuzz. These nano-structures are formed under high flux helium bombardment at low energies and at temperatures in the range of $1000 - 2000\,\mathrm{K}$ [3, 4, 5]. Due to the high porosity of these structures the heat transfer is reduced, which could lead to melting of the PFM, especially in the divertor region of a nuclear fusion device and is therefore highly unwanted [3, 5, 6]. Furthermore sputtering of such nanostructures by ion bombardment is less understood and therefore more investigations are needed.
Figure 1 shows the schematics of sputtering a nanostructured surface. If a projectile beam hit a surface under normal incidence, the so called local angle of incidence Θ differs considerably, which influences the sputtering behaviour [7]. With increasing surface roughness redeposition of sputtered material will become more dominant, causing further surface morphology modifications [8]. Nanostructures on a surface can cause shadowing of underlying structures, but also severe redeposition of sputtered material. The sputtering behaviour of

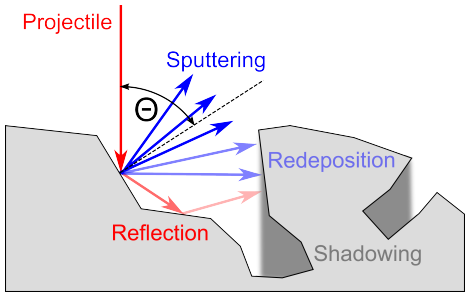

Figure 1: Schematics of sputtering of a nanostrucured surface. Projectile refelction, sputtered particles redeposition and shadowing of underlying areas may occur.

nanostructured surfaces, like W-fuzz is, therefore, complicated and further investigations are essential. Due to the fact that the collision cascade cannot evolve completely in such nanostructured morphologies, such investigations are also of high interest in basic sputtering research.
The objective of this work was to investigate the erosion behaviour of nanostrucutred tungsten in detail, by using the TU Wien quartz crystal microbalance technique (QCM) in a particle catcher configuration and under well defined laboratory conditions [9]. With this technique sputtered particles distributions can be measured, by varying the relative position of the QCM-catcher.
Furthermore, the state-of-the-art 3D Monte Carlo binary collision approximation (MC-BCA) code TRI3DYN was used. It allows sputter modelling of any

3D surface, as well as nanostructured morphologies [10]. The modelled dynamic erosion behaviour (in particular the sputtered particles distributions as well as the surface morphologies) was compared to the experimental results. Surface morphologies changes were experimentally investigated by pre- and post scanning electron microscopy (SEM) analysis of the W-Fuzz samples.

2. Material and Methods

2.1. Sample Preparation and Analysis

The W-fuzz samples were produced at the Forschungszentrum-Jülich (FZJ), by using the PSI-2 linear plasma device [11]. Polycrystalline W bulk material was exposed to a He plasma at temperatures beyond 1000 K. The exposure to this low energy He ion flux of about $10^{22}\,\mathrm{m^{-2}s^{-1}}$ leads to the growth of nanostructured W [3]. Sample analysis by SEM measurements at the Helmholtz-Zentrum-Dresden-Rossendorf (HZDR) and FZJ revealed a clearly nanostructured W surface. Figure 2 shows a typical SEM image of one of the W-fuzz samples. Analysing this image by using the software ImageJ an areal density of 50% and a string thickness of about 40 nm could be evaluated [12].

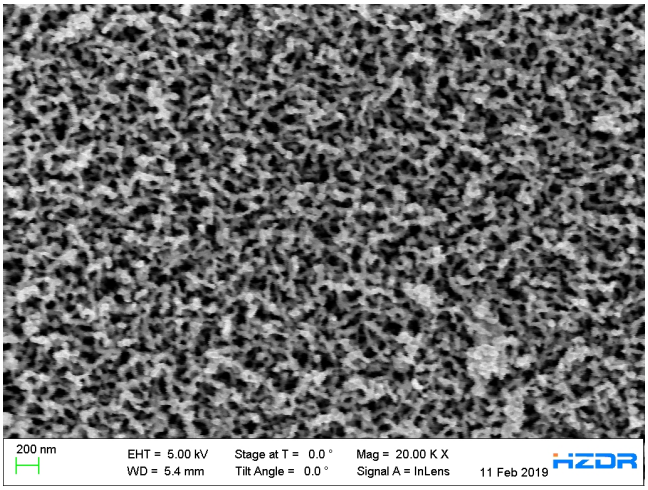

Figure 2: A top-view SEM image of a W-fuzz sample displaying the fuzzy nanostructures. An areal density of 50% and a string thickness of about 40 nm could be evaluated.

The SEM image in figure 3 shows a focused ion beam (FIB)-cut SEM measurement into a virgin W-fuzz sample. A Ga ion beam with 30 keV was used to cut through the fuzz material. The image is tilted by 54° revealing a cross section through the W-fuzz. A fuzz height of about 2 μm can be estimated.

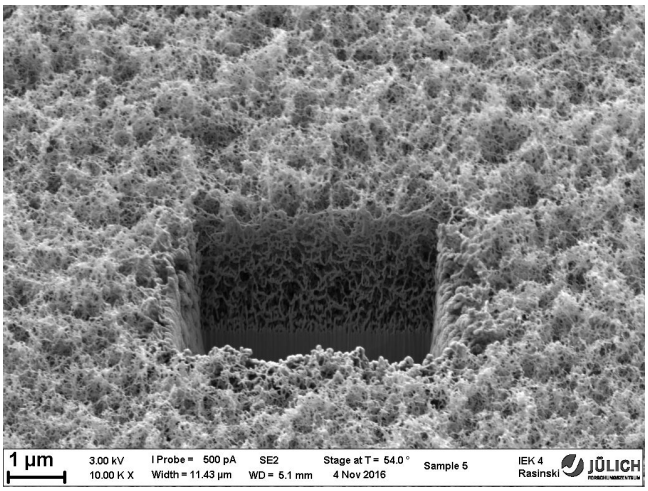

Figure 3: SEM image of the W-fuzz sample with a FIB-cut spot, tilted by 54°. A Ga ion beam was used, with 30 keV to cut through the fuzz material, revealing the underlying nanostructure material. The thickness of the fuzz layer is about 2 μm can be assessed.

2.2. Experimental approach

The TU Wien QCM technique is a highly sensitive experiment for evaluating sputtering yields. In the classic configuration a quartz crystal is coated with a thin film of the material to be investigated. By bombarding this crystal with a well defined ion beam, the sputtering yield of the material can be determined by measuring the change of the resonance frequency [13, 8, 14, 15, 16, 17]. A drawback of this technique is, that it is limited to a material film thickness of some 100 nm. The TU Wien QCM technique in particle catcher configuration is an upgrade of the classic configuration. It is an ideal tool to investigate the sputtering behaviour of nearly any target. It allows in situ erosion measurements and evaluation of sputtered particles distributions [9]. A schematics of the experimental setup can be seen in figure 4. A sputter ion source (Specs IQE12/38 with Wien filter) provides a mass filtered and focused Ar^{1+} ion beam, with 2 keV and an average ion flux of $10^{17}\,m^{-2}s^{-1}$. An built-in focusing and scanning device allows precise focussing and ion beam scanning. The ion current was measured by using a Faraday-cup, positioned on the sample holder. A XYZΦ stage allows precise positioning of the sample-holder as well as the macroscopic angle of incidence α of the ions. The catcher-QCM is mounted on a linear stage, allowing a precise adjustment of the distance d and the relative position Δx of the catcher with respect to the impact position of the ion beam. In addition it is ensured that the catcher QCM is always positioned parallel to the ion beam. For more details of the QCM technique in general the reader is referenced to [9, 13, 14].

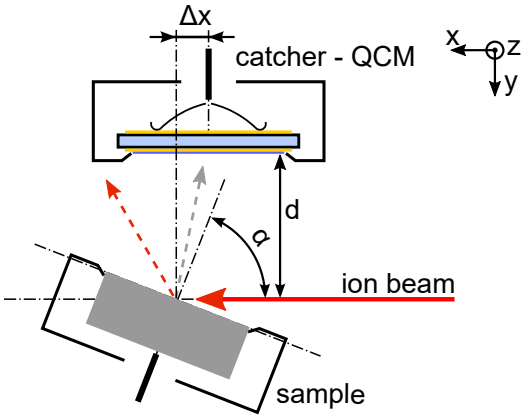

Figure 4: Schematics of the experimental setup. An Ar^{1+} ion beam originating from a sputter ion source hits a sample under the angle of incidence α. A fraction of the sputtered particles from the sample hit the catcher QCM, which is located at a variable distance d and position Δx relative to the center of the sample (indicated as gray arrow). Scattered projectiles (red dashed arrow) may also hit the catcher surface, causing sputtering and a therefore reducing the signal. By stepwise adapting the relative position Δx the sputtered particles distribution can be evaluated.

Pre- and post irradiation analysis of the nanostructured W-fuzz samples were performed by using SEM at the FZJ as well as at the HZDR research centres.

2.3. Simulation approach

The state-of-the art 3D sputter modelling software TRI3DYN [10] represents an enhanced version of TRIDYN [18], expanded in full 3D. It is based on a monte-carlo (MC) code, using the binary-collision-approximation (BCA) and allows to evaluate erosion yields, sputtered and scattered particles distribution as well as the erosion dynamics of a sputter target. TRIDYN is limited to one dimension only (depth). Here the sputter target is set up in layers with infinite lateral expansion. These layers can be predefined with different elemental concentrations. A drawback of this approach is, that only flat samples can be modelled. TRI3DYN extended this principle, by subdividing these layers into small cubic volumes with a defined elemental density. These volumes are called 'voxels' and can be stacked on top of each other, allowing to create nearly any 3D structure. Other codes like SDTrimSP-2D and SDTrimSP-3D are based on the same principle [19, 7, 20].
In order to avoid inaccuracies due to discretization of a real sputter target, the voxel resolution should be high. On the other hand a high amount of voxels increases the computation time tremendously, therefore the lateral expansion of the modelled object is limited. A good compromise is to use a voxel size, which is about the length of the expected collision cascade [8].
The code uses so called 'pseudoatoms' as projectiles, wich represent a certain amount of real projectiles. Due to the fact that TRI3DYN is a MC code, a higher statistical accuracy can only be achieved, by using a high pseudoatom

number. We used a pseudoatom to real atom factor of 1 for evaluation of static sputtered and scattered particles distribution static modelling, where changes in the target are suppressed. For dynamic erosion modelling a factor of 200 needed to be used in order to keep the computing time within limits. The dynamic modelling includes also voxel relaxation procedures. After a certain amount of modelled pseudoatoms the voxel elemental density is verified. If it gets too high material will flow to a neighbouring voxel with lower density. This also happens if the density gets too low, where the residual material will be assimilated to a neighbouring voxel, causing the deletion of this voxel. For a more precise explanation of the relaxation procedures and the exact function of the TRI3DYN code, the reader is referred to [10, 18].

2.3.1. Creation of a W-fuzz model

To create an appropriate W Fuzz target input for TRI3DYN informations from SEM images were used. By analysing these images (figure 2 and 3) using the software ImageJ an areal density of 50% and a string thickness of about 40 nm was evaluated. By using these two parameters a 'random-walk' algorithm grows single W strings from a flat surface, where the starting point as well as the polar and azimuthal direction were randomly chosen. After a grow length of two times the string thickness the grow-direction is again randomly varied. As soon as such a string reaches a maximum height a new string starts to grow. This procedure is repeated until the measured areal density of 50% is reached. Figure 5 shows the randomly generated W-fuzz target for TRI3DYN, which was used for the modelling. It should also be noted, that periodic boundary conditions are used in both lateral Y and Z directions. As elemental composition pure W was assumed. Unfortunately the assessed total W-fuzz height from figure 3 of 2 μm is to big to be modelled, therefore we are limited to a total fuzz volume of $0.5 \times 0.5 \times 0.5\,\mu\mathrm{m}^3$.

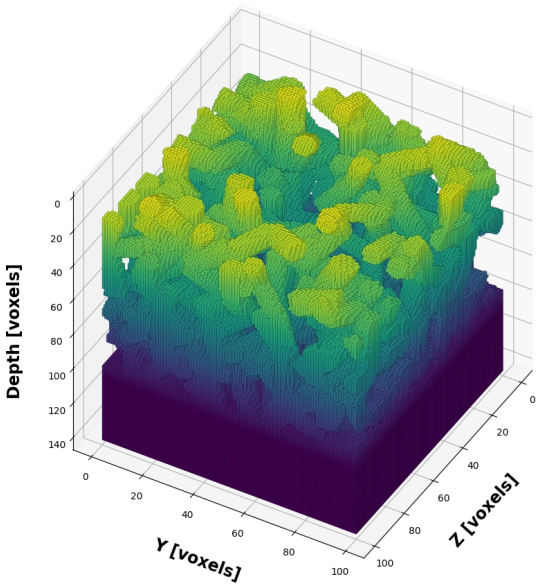

Figure 5: Randomly generated W-fuzz structure, as input for TRI3DYN. By using areal coverage density as well as string thickness information from SEM images from real W-fuzz, this structure was generated. The color code is depth dependent and used to highlight the 3D structure. A voxel size of $50 \times 50 \times 50$ Å^3 was used allowing to model a total fuzz volume of $0.5 \times 0.5 \times 0.5\,\mu$m^3. Below this fuzz structure 40 filled voxel layers of pure W were added to prevent transmission through the bottom. The code uses periodic boundary conditions in both lateral Y and Z directions.

2.3.2. Reconstruction of the QCM catcher measurements

By using a correct sputtered and scattered particles spacial-distribution f_{sp} the expected TU Wien QCM catcher signal can be predicted (for more details see reference [9]). Taking into account the geometric layout from figure 4, including the angle of incidence of the primary ion beam α, the catcher distance d, ion beam scanning, as well as the sensitivity s of the quartz crystal, the QCM-catcher signal Y_{total} can be calculated for every Δx position according to formula 1:

$$Y_{total}(\Delta x, \alpha, d) = Y_c(\Delta x, \alpha, d) - Y_{sp}(\Delta x, \alpha, d) \tag{1}$$

Y_c is the yield of catched sputtered particles and Y_{sp} the sputter yield at the catcher, caused by scattered projectiles from the ion beam.

$$Y_c(\Delta x, \alpha, d) = \sum_{x,y} \sum_{\Omega} f_{sp,sp}(\Omega, \Delta x, x, y) \cdot s(\Omega, \alpha, d) \tag{2}$$

$$Y_{sp}(\Delta x, \alpha, d) = \sum_{x,y} \sum_{\Omega} \sum_{E} F_{sp,sc}(\Omega, \Delta x, x, y) \cdot s(\Omega, \alpha, d) \tag{3}$$

$$F_{sp,sc}(\Omega, \Delta x, x, y) = \sum_{E} f_{sp,sc}(\Omega, \Delta x, x, y, E) \cdot Y_{Ar \to W}(E) \tag{4}$$

Y_c and Y_{sp} are calculated according to formula 2 and 3. At a given QCM catcher position the spacial distribution f_{sp} is weighted with the radial sensitivity of the quartz s and numerically integrated over solid angle Ω, as well as the ion beam scan area along x and y. For Y_{sp} the energy and therefore the sputtering yield of the scattered particles is included in the spacial distribution $F_{sp,sc}$, as can be seen in equation 4. The energy dependence of the sputtering yield $Y_{Ar\rightarrow W}(E)$ was evaluated via a separate modelling, assuming a flat W surface.

3. Results

The W-fuzz samples were stepwise exposed to Ar^{1+} irradiation at 2 keV. The size of the two fluence steps are listed in table 1. After each step the QCM-catcher technique was used to measure the sputtered particle distribution (figure 15).

Table 1: total applied fluences to W-fuzz sample after a particular step

step no.	Ar^{1+} fluence $[10^{20}\,m^{-2}]$
1	8.6 ± 0.9
2	176 ± 18

After fluence step 1 and 2, SEM images of the irradiated W-fuzz were made. In figure 6 the surface of a W-fuzz after step 1 is shown. The nanostructures are visible, but the formation of grooves in the direction of the ion beam is already starting. Figure 7 shows a top-view SEM image after step 2 near a transition region from unsputtered to the sputtered W-fuzz. The lower left part of the image shows the typical W-fuzz nanostructures, while the upper right shows a scaly structure. Here small periodic cones are visible, which are aligned in the direction of the incident ion beam. Figure 8 shows an enlargement of this scaly structure. The scales have a thickness of 216 ± 48 nm and a length of 390 ± 141 nm (evaluated by using the software ImageJ [12]). An inclined SEM image of the same sample (figure 9) facing directly the hills, reveals that the cones are nearly round at the origin, with a diameter of 307 ± 73 nm. In order to check if there is still a W-fuzz structure under this scaly surface, again a FIB-cut was made. In figure 10 the resulting SEM image can be seen. Although during the FIB-cutting process melting at the edges is visible, an underlying W-fuzz structure can no longer be found.

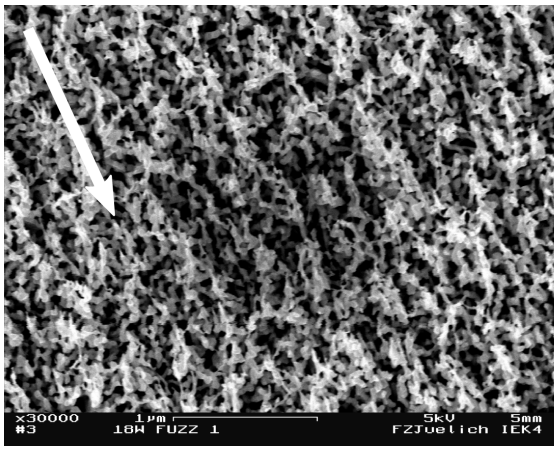

Figure 6: SEM image of the W-fuzz sample, showing the surface structure after an Ar^{1+} fluence of $8.6 \times 10^{20}\,m^{-2}$. The direction of the ion beam is indicated by the white arrow. Fuzzy nanostructures are still visible, but show an alignment in the direction of the ion beam.

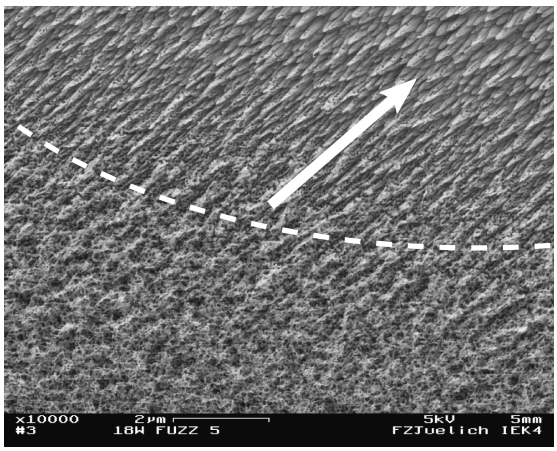

Figure 7: SEM image of the W-fuzz sample, showing a transient region from unsputtered (lower left) to sputtered area (upper right) after an Ar^{1+} fluence of $1.76 \times 10^{22}\,m^{-2}$. The boundary region is indicated by a dashed white line. The sputtered region show a scale-like structure, where the tips are pointing in the direction of the incident ion beam (beam direction indicated as white arrow).

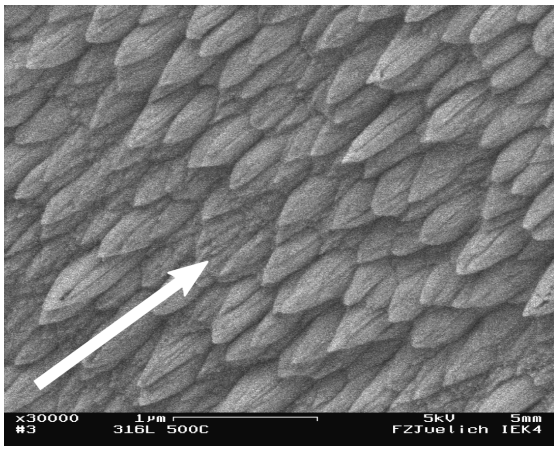

Figure 8: Magnified SEM image of the sputtered W-fuzz sample after a total Ar^{1+} fluence of $1.76 \times 10^{22}\,m^{-2}$. Small periodic cones similar to fish scales are visible, aligned in the direction of the incident ion beam (indicated as white arrow).

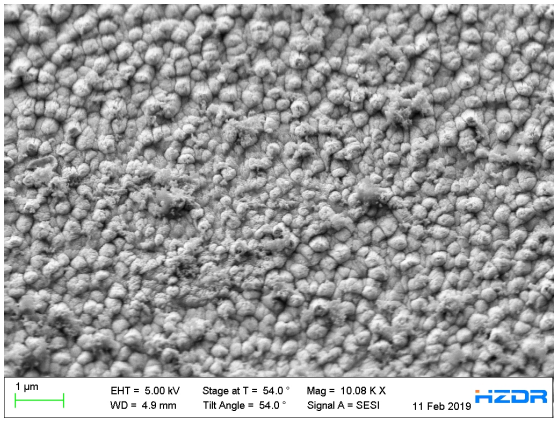

Figure 9: Tilted SEM image of the sputtered W-fuzz sample after an Ar^{1+} fluence of $1.76 \times 10^{22}\,m^{-2}$. A tilt angle of 56 degree was used, which is close to the ion beam angle of incidence of 60 degree. The cones of the scaly surface point in the direction of the viewer.

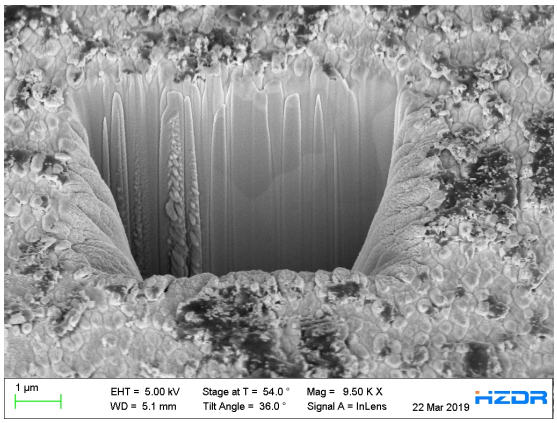

Figure 10: FIB-Cut SEM image of the sputtered W-fuzz sample after an Ar fluence of $1.76 \times 10^{22}\,\mathrm{m}^{-2}$. No underlying Fuzz structure is visible.

3.1. TRI3DYN modelling results

TRI3DYN was used to compare a perfectly flat surface to the W-fuzz model surface from figure 5. Figure 11 shows the results of sputtered particles distribution at an angle of incidence of 60° (with respect to the surface normal). In total 2.5×10^7 pseudoparticles were modelled, to ensure a good statistics. While the flat target in figure 11(a) shows a clear forward sputtering and a singe knock-on peak at around $-50°$, the fuzz target shows a pronounced back-sputtering in the direction of the incident ion beam, peaking at around 35°. Comparing the results of scattered Ar projectiles distributions in figure 12 show a very similar outcome. While the flat target in figure 12(a) shows a clear forward scattering and a single scattering peak at around $-30°$, the fuzz target shows a much broader distribution, slightly pronounced back-scattering in the direction of the incident ion beam and peaking also at around 35°. Here a single-scattering peak is visible too at $-30°$. All presented distributions are normalized to the total number of sputtered/scattered pseudoparticles.

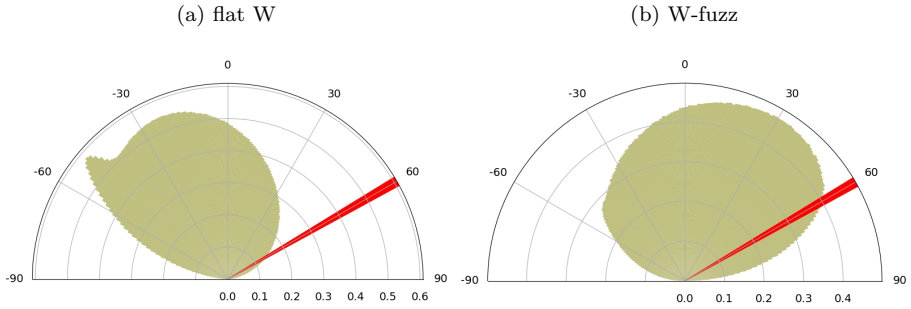

Figure 11: Result of sputtered particles distribution modelling with TRI3DYN, using a binning of 1°. The Ar^{1+} ion beam is marked as red arrow and hits the surface under an angle of incidence of 60° (with respect to the surface normal at 0°). In (a) the distribution of a flat W target can be seen, while in (b) the distribution of a nanostructured W-fuzz target is displayed.

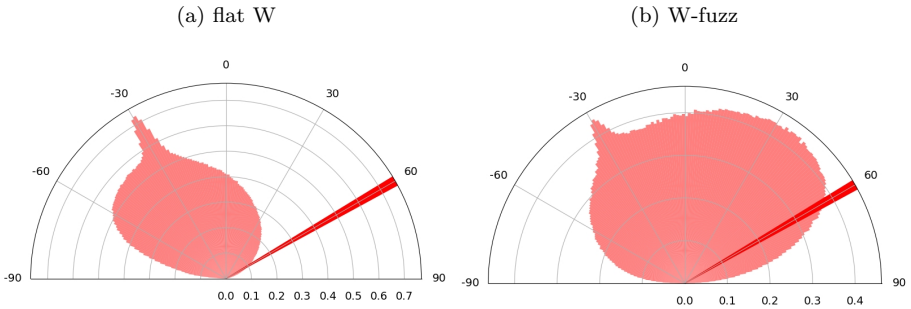

Figure 12: Result of scattered projectile distribution modelling with TRI3DYN. In (a) the distribution of a flat W target can be seen, while in (b) the distribution of a nanostructured W-fuzz target is displayed. The angle of incidence of the incident ion beam was 60° (with respect to the surface normal) and is marked as red arrow.

TRI3DYN also allows dynamic erosion modelling of a nanostructured surface. The results of a simulated erosion of the initial W-fuzz structure from figure 5 after an Ar fluence of $1 \times 10^{21}\,\mathrm{m}^{-2}$ at 2 keV Ar^{1+} impact energy can be seen in figure 13. The ion beam hit the surface under an angle of incidence of 60° (with respect to the surface normal). The initial W-fuzz nanostructure is still observable but the formation of grooves in direction of the ion beam begins to start. Some voxel-clusters stay at elevated positions, pointing out the limit of the underlying physical model, but it must be noted that the code used periodic boundary conditions in both Y and Z coordinates.

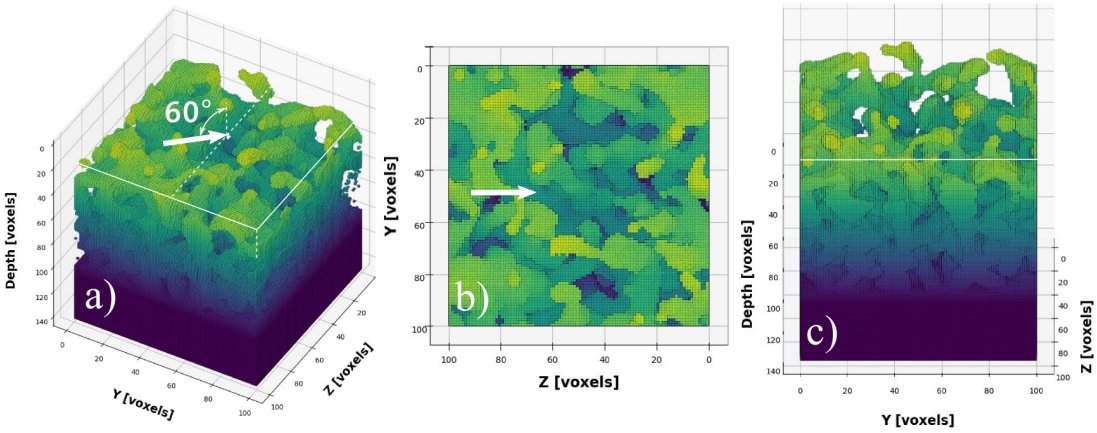

Figure 13: Result of dynamic erosion modelling with TRI3DYN, after a simulated fluence of $1 \times 10^{21}\,\mathrm{m}^{-2}$. The fuzz structure is still visible, but a slight alignment in the direction of the incident ion beam (indicated as white arrow) can be seen. In (a) the resulting 3D structure can be seen. (b) shows a top view of this structure and in (c) the structure is inclined by 60 degrees so that the peaks of the scales point directly towards the observer and the incident ion beam. The solid white lines mark the edge of the surface. The code uses periodic boundary conditions in both Y and Z coordinates and voxel-size of $50 \times 50 \times 50\,\mathrm{Å}^3$ was used.

In figure 14 the modelled W-fuzz structure after a simulated Ar fluence of $1.7 \times 10^{22}\,\mathrm{m}^{-2}$ is shown. The surface changed to a scaly-like morphology, where the tips point in the the direction of the incident ion beam. By including the periodic boundary conditions in both lateral Y and Z direction a scale length of $296 \pm 102\,\mathrm{nm}$ can be seen. The thickness of the scales at its origin can be evaluated as $76 \pm 46\,\mathrm{nm}$ (by using the software ImageJ [12]).

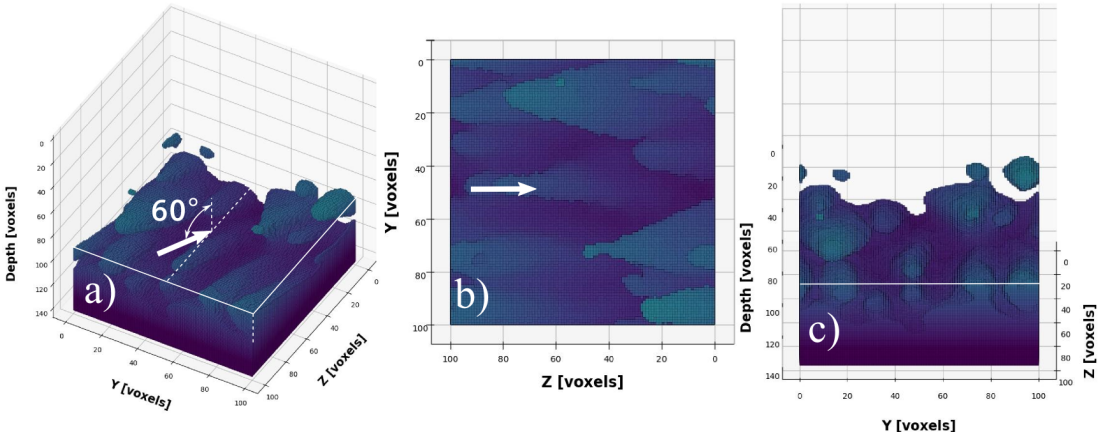

Figure 14: Result of dynamic erosion modelling with TRI3DYN, after a simulated fluence of $1.7 \times 10^{22}\,\mathrm{m}^{-2}$, revealing a cone-like surface morphology pointing directly in the direction of the incident Ar^{1+} ion beam (indicated as white arrow). In (a) the resulting surface structure can be seen. (b) shows a top view of this structure and in (c) the structure is inclined by 60 degrees so that the peaks of the scales point directly towards the observer and the incident ion beam. The solid white lines mark the edge of the surface.

Comparing the surface morphology results of the TRI3DYN code to the SEM images reveal good agreement. After a Ar fluence of $8.6 \times 10^{20}\,\mathrm{m}^{-2}$ the W-fuzz structure is still visible, as can be seen in the SEM image of figure 6 and can be confirmed by TRI3DYN (figure 13). Although the lateral expansion of the W-fuzz model for TRI3DYN is only $0.5 \times 0.5\,\mu\mathrm{m}^2$, a slight alignment of the surface structure in the direction of the incident ion beam can be observed.
After an Ar fluence of $1.7 \times 10^{22}\,\mathrm{m}^{-2}$ no W-fuzz structures can be found, neither in the SEM images (figure 8) nor in the TRI3DYN modelling results (figure 14), despite the fact that only $0.5\,\mu\mathrm{m}$ ($50\,\text{Å} \times 100$ voxels) of fuzz have been sputtered away. A scaly structure is revealed in the experiment as well as in TRI3DYN. The length and thickness of the resulting scales in TRI3DYN is comparable but somewhat smaller compared to the SEM results, which can likely be attributed to the smaller fuzz volume in the model.

3.2. QCM catcher results and comparison to modelling

Figure 15 and figure 16 present the total QCM catcher yields at different Δx positions. In figure 15 the measured QCM catcher yield over Δx can be seen for a flat W sample as well as a W-fuzz sample in initial state and after certain Ar^{1+} irradiation steps with 2 keV under an angle of incidence of 60°. The applied fluences in the different steps are given in table 1.

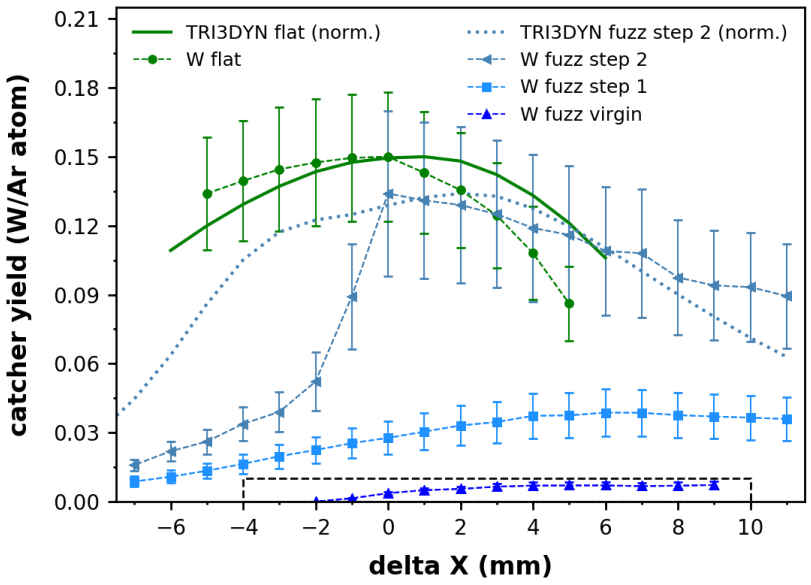

Figure 15: QCM Catcher measurement results (symbols) of a flat W surface (green) as well as a W-fuzz target (blue) and comparison to modelling with TRI3DYN. The flat sample show a maximum catcher yield at $\Delta x = 0\,\mathrm{mm}$, while the virgin fuzz target and the fuzz target after fluence step 1 show a smaller catcher yield, peaking around $\Delta x = 6\,\mathrm{mm}$. Further erosion of the fuzz target leads to an approach of the fuzz sample results to the flat target data. TRI3DYN can reproduce the catcher yield of a flat target and also the W-fuzz target after fluence step 2, although some deviations at negative Δx values are still observable.

The flat sample revealed a distribution with a maximum at $\Delta x = 0\,\mathrm{mm}$ with a total catcher yield of $0.15 \pm 0.03\,\mathrm{W/Ar}$. The virgin fuzz sample instead, shows a broad distribution with a maximum around $\Delta x = 6\,\mathrm{mm}$ and a total catcher yield with $0.007 \pm 0.001\,\mathrm{W/Ar}$, which is only about 5% of the yield of the flat sample. A continuous increase in the W-fuzz catcher yield after each fluence step can be observed. The measured total catcher yield gradually approaches the distribution of the flat sample, although deviations at negative Δx values remain, which may be caused by the scaly structure formation.
In figure 16 an enlargement of the black dashed area from figure 15 can be seen, highlighting the virgin W-fuzz behaviour. The distribution of the initial W-fuzz target peaks at around $\Delta x = 6\,\mathrm{mm}$. In the inset of figure 16 a precise setup schematics at this Δx position is shown, where the surface normal of the fuzz sample is pointing towards the center of the catcher QCM, indicating that preferential sputtering in the direction of the surface normal occurs.

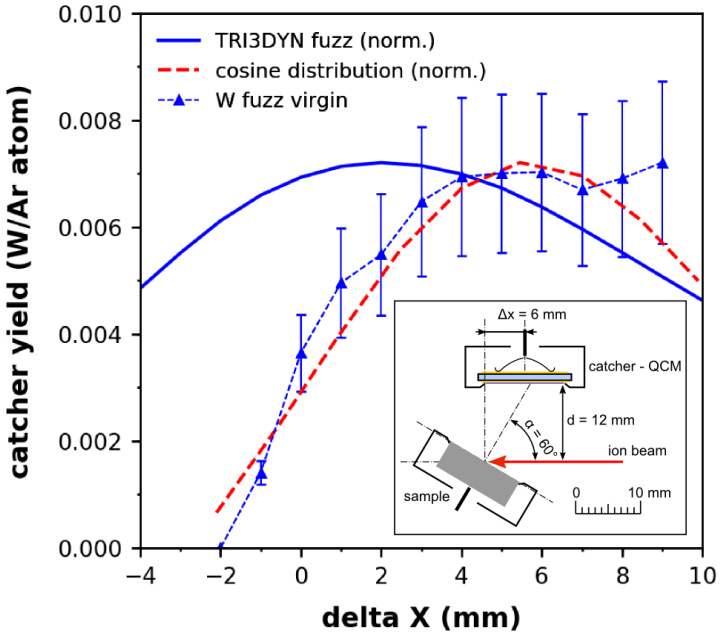

Figure 16: QCM Catcher measurement results of a virgin W-fuzz target and comparison to modelling with TRI3DYN as well to a numerical fit using a pure cosine distribution. The virgin fuzz target shows a maximum catcher yield of 0.007 ± 0.001 W/Ar, around $\Delta x = 6$ mm. In the inset a precise setup schematics at $\Delta x = 6$ mm is shown, where the surface normal of the sample points towards the center of the catcher QCM, indicating that preferential sputtering in the direction of the surface normal occurs. The TRI3DYN results show a maximum at $\Delta x = 2$ mm. By using the cosine distribution from equation 5 the measured trend can be reproduced. The TRI3DYN result and the cosine distribution were normalized to the maximum of the measured total catcher yield.

By using the sputtered and scattered particle distributions from TRI3DYN, an attempt was made to reconstruct the the total catcher yield, according to formula 1. While TRI3DYN can quantitatively reproduce the catcher signal of a flat target (solid green line in figure 15), the modelling of the fuzz target shows a deviation of the maximum position, as can be seen in figure 16 (solid blue line), where a maximum at $\Delta x = 2$ mm was found. By using the sputtered and scattered particle distributions from TRI3DYN after a simulated erosion of $1.7 \times 10^{22}\,\mathrm{m}^{-2}$ (surface from figure 14) the catcher yield reconstruction agrees well with the measurement at $\Delta x \geq 0$ mm (compare with figure 15).
It is interesting to see that by assuming a pure cosine distribution of sputtered particles including a polar shift of 45° (equation 5) the initial W-fuzz behaviour can be reproduced, as shown as red-dashed line in figure 16.

$$f_{sp,sp}(\Omega(\Theta,\Phi)) = cos(\pi/4 + \Theta) \tag{5}$$

By using the QCM technique in classic configuration (see reference [13, 16]), by directly irradiating a quartz crystal with a thin and flat W layer deposited on

it, a sputtering yield of 1.41 ± 0.26 W/Ar is measured for 2 keV Ar^{1+} impact at 60°. Using the data of the catcher measurements, where we find that the fuzz catcher signal is a factor 20 lower and including a geometric correction factor including the increased target-catcher distance at $\Delta x = 6$ mm, a W-fuzz sputtering yield of 0.08 ± 0.05 W/Ar can be estimated.

4. Discussion

The QCM-catcher technique reveals a sputtered particle distribution of W-fuzz, which peaks in the direction of the samples surface normal and has an approx. 20 times lower catcher yield as compared to a flat W sample (see figure 15 and 16. Other groups confirm a W-fuzz sputtering yield, which is one order of magnitude lower compared to a flat target [6]. This indicates that a nanostructured surface causes severe redepostion of sputtered material, leading to a much lower sputtering yield. Furthermore sputtered particles may preferably exit the fuzz-surface in the direction of the incident ion beam, where a path to the surface is open [6].

After eroding the W-fuzz sample by applying a high Ar fluence the measured total catcher yield approaches the one of a smooth sample, nevertheless deviations at negative Δx values are observable. The SEM measurements of the fuzz samples after irradiation show the formation of a scaly structure facing in the direction of the incident ion beam. This structures still cause redeposition of sputtered material and may shield the QCM catcher at negative Δx values.

The 3D-MC-BCA code TRI3DYN allows sputter modelling of such nanostructured surfaces, by using so called voxels. The dynamic erosion of a W-fuzz structure and the formation of a scaly structure can be well reproduced, as can be seen by comparing figure 14 to 8. The revealed sputtered and scattered particle distributions confirm that a nanostructured surface causes 'backward'-sputtering and scattering in the direction of the incident ion beam. By using these distributions to reconstruct the QCM catcher measurements a deviation is observable, as demonstrated in figure 15, 16. This deviation is caused by an overestimation of sputtered and scattered particles in forward direction. This may be caused by a too simple W-fuzz model. In TRI3DYN every voxel is assumed to include pure W with a surface binding energy of a bulk material, which may not hold true for a nanostructure like W-fuzz. Furthermore effects like surface tension are not yet included in the code. Nevertheless our comparison points out the capability of MC-BCA codes. Smaller voxel sizes and bigger modelling volumes may increase the accuracy at the cost of computation time.

5. Conclusion and Outlook

The TU Wien QCM-catcher technique is a powerful tool to investigate the sputtering properties of a target of nearly any morphology. By irradiation of a W-fuzz sample with Ar^{1+} ions at 2 keV and 60° angle of incidence backward sputtering was observed and a W-fuzz sputtering yield of 0.08 ± 0.05 W/Ar could

be estimated. After continuous irradiation an increase in the catcher yield was observed as well as a shift of the sputtered particles distribution, approaching the distribution of a flat W-target. SEM measurements reveal a scaly surface morphology, facing in the direction of the ion beam.
TRI3DYN as a full 3D-MC-BCA code allows modelling of nearly any surface morphology and the results of W-fuzz modelling is very promising, although some deviations to experiments are still observable. The formation of a scaly structure after continuous Ar irradiation can be reproduced and shows the strength of this modelling method.
In a nuclear fusion device contamination of the fusion plasma by high Z materials is highly unwanted, due to the increased radiation cooling. W-fuzz was feared to increase this contamination, but our measurements show that the sputtering yield is much lower than flat W. Therefore this should not happen, although at elevated temperatures the sputtering behaviour can be different, making further investigations necessary.
Nanostructured surfaces like W-fuzz may also be used to improve solar cells, due to their excellent light absorption properties and the increased surface area of the fuzz could improve chemical reactions and may be used in catalytic converters.

Acknowledgements

The authors are grateful to Michael Schmid (IAP, TU Wien) for his continued support with the QCM electronics and to Richard A. Wilhelm (IAP, TU Wien) for valuable discussions.
This work has been carried out within the framework of the EUROfusion Consortium and has received funding from the Euratom research and training programme 2014–2018 and 2019-2020 under grant agreement No 633053. The views and opinions expressed herein do not necessarily reflect those of the European Commission. Financial support has also been provided by KKKÖ (commission for the coordination of fusion research in Austria at the Austrian Academy of Sciences – ÖAW).
The computational results presented have been achieved in part using the Vienna Scientific Cluster (VSC).

References

[1] BREZINSEK, S. et al., Nuclear Fusion **57** (2017) 116041.

[2] PITTS, R. A. et al., Journal of Nuclear Materials **415** (2011) S957.

[3] SHIN, K. et al., Nuclear Fusion **49** (2009) 095005.

[4] BALDWIN, M. J. et al., Journal of Nuclear Materials **415** (2011) S104.

[5] BALDWIN, M. J. et al., Nuclear Fusion **48** (2008) 035001.

[6] NISHIJIMA, D. et al., Journal of Nuclear Materials **415** (2011) S96.

[7] STADLMAYR, R. et al., Nuclear Instruments and Methods in Physics Research Section B: Beam Interactions with Materials and Atoms **430** (2018) 42.

[8] STADLMAYR, R. et al., Physica Scripta (2019) in print.

[9] BERGER, B. M. et al., Nuclear Instruments and Methods in Physics Research Section B: Beam Interactions with Materials and Atoms **406** (2017) 533.

[10] MöLLER, W., Nuclear Instruments and Methods in Physics Research Section B: Beam Interactions with Materials and Atoms **322** (2014) 23.

[11] KRETER, A. et al., Fusion Science and Technology **68** (2015) 8.

[12] SCHNEIDER, C. A. et al., Nature Methods **9** (2012) 671.

[13] HAYDERER, G. et al., Review of Scientific Instruments **70** (1999) 3696.

[14] GOLCZEWSKI, A. et al., Nuclear Instruments and Methods in Physics Research Section B: Beam Interactions with Materials and Atoms **267** (2009) 695.

[15] BERGER, B. M. et al., Nuclear Instruments and Methods in Physics Research Section B: Beam Interactions with Materials and Atoms **382** (2016) 82.

[16] DOBES, K. et al., International Journal of Mass Spectrometry **365-366** (2014) 64.

[17] BERGER, B. M. et al., Nuclear Materials and Energy **12** (2017) 468.

[18] MöLLER, W. et al., Nuclear Instruments and Methods in Physics Research Section B: Beam Interactions with Materials and Atoms **2** (1984) 814.

[19] MUTZKE, A. et al., Sdtrimsp-2d: Simulation of particles bombarding on a two dimensional target-version 2.0, Report, Max-Planck-Institut für Plasmaphysik, 2013.

[20] VON TOUSSAINT, U. et al., Physica Scripta **T170** (2017) 014056.